


# A Survey of Precipitation-Induced Atmospheric Cold Pools over Oceans and Their Interactions with the Larger-Scale Environment

Paquita Zuidema<sup>1</sup>  · Giuseppe Torri<sup>2</sup> · Caroline Muller<sup>3</sup> · Arunchandra Chandra<sup>1</sup>

Received: 2 April 2017 / Accepted: 29 October 2017 / Published online: 14 November 2017  
© The Author(s) 2017. This article is an open access publication

**Abstract** Pools of air cooled by partial rain evaporation span up to several hundreds of kilometers in nature and typically last less than 1 day, ultimately losing their identity to the large-scale flow. These fundamentally differ in character from the radiatively-driven dry pools defining convective aggregation. Advancement in remote sensing and in computer capabilities has promoted exploration of how precipitation-induced cold pool processes modify the convective spectrum and life cycle. This contribution surveys current understanding of such cold pools over the tropical and subtropical oceans. In shallow convection with low rain rates, the cold pools moisten, preserving the near-surface equivalent potential temperature or increasing it if the surface moisture fluxes cannot ventilate beyond the new surface layer; both conditions indicate downdraft origin air from within the boundary layer. When rain rates exceed  $\sim 2 \text{ mm h}^{-1}$ , convective-scale downdrafts can bring down drier air of lower equivalent potential temperature from above the boundary layer. The resulting density currents facilitate the lifting of locally thermodynamically favorable air and can impose an arc-shaped mesoscale cloud organization. This organization allows clouds capable of reaching 4–5 km within otherwise dry environments. These are more commonly observed in the northern hemisphere trade wind regime, where the flow to the intertropical

---

✉ Paquita Zuidema  
pzuidema@miami.edu

Giuseppe Torri  
torri@fas.harvard.edu

Caroline Muller  
carolinemuller123@gmail.com

Arunchandra Chandra  
achandra@miami.edu

<sup>1</sup> Rosenstiel School of Marine and Atmospheric Science, University of Miami, 4600 Rickenbacker Causeway, Miami, FL 33149, USA

<sup>2</sup> Department of Earth and Planetary Sciences, Harvard University, 20 Oxford St., Cambridge, MA 02138, USA

<sup>3</sup> CNRS Laboratoire d'Hydrodynamique de l'École Polytechnique, Palaiseau, France

convergence zone is unimpeded by the equator. Their near-surface air properties share much with those shown from cold pools sampled in the equatorial Indian Ocean. Cold pools are most effective at influencing the mesoscale organization when the atmosphere is moist in the lower free troposphere and dry above, suggesting an optimal range of water vapor paths. Outstanding questions on the relationship between cold pools, their accompanying moisture distribution and cloud cover are detailed further. Near-surface water vapor rings are documented in one model inside but near the cold pool edge; these are not consistent with observations, but do improve with smaller horizontal grid spacings.

**Keywords** Convective cold pools · Tropical convection · Shallow cumulus convection

## 1 Introduction

Cold pools are defined by the American Meteorological Society (AMS) as “a region or pool of relatively cold air surrounded by warmer air,” or, “any large-scale mass of cold air” (Glickman 2000). In one example, nighttime radiative cooling of a land surface can create a near-surface cold pool of air. Over the open ocean, far from land, the cooling of near-surface air is arguably exclusively caused by the partial evaporation of precipitation within subsaturated air. This precipitation can be liquid or solid, though in subtropical and tropical regions the precipitation is entirely liquid near the surface. The precipitation-induced downdrafts introduce denser air underneath warmer, lighter environmental air, giving rise to a density current. The increased surface pressure establishes a horizontal pressure gradient force that drives the cold pool air outward, establishing an outflow boundary known as a gust front. The air inside the cold pool is less able to support surface-based buoyancy-driven convection. The gust front itself behaves as a material surface, and air moving over the gust front can encourage further secondary convection through mechanical lifting and anomalous buoyancy. Such convectively produced atmospheric cold pools are typically observed to span 10–200 km in diameter, and to last for less than a day, after which they lose their individual identity to the large-scale or synoptic flow. This range of sizes and lifetimes identifies them as mesoscale features, although cold pools are often embedded in and can help define the edges of larger synoptic systems (e.g., squall lines or hurricane rainbands).

Although the latent cooling from evaporation of precipitation is necessary for creating a cold pool, not all precipitation leads to well-defined cold pools at the bottom of the atmosphere. Precipitative downdrafts are driven by both condensate loading and evaporation, and, if the resulting downdraft is not strong enough to reach the surface, elevated patches of moist, cool air remain. These most likely will not fit the AMS cold pool definition, in that they are unlikely to be completely surrounded by warmer air. One example, common in stratocumulus clouds because of their relatively smaller precipitation drop sizes (e.g., Wood 2005b), is light precipitation (drizzle) evaporating below cloud base (e.g., Wood 2005a). The local cooling can serve to destabilize the subcloud layer and reinforce the updrafts in stratocumulus clouds (e.g., Feingold et al. 1996) and can also be visualized in lower-level scud clouds. In the shallow cumulus regime, such an elevated enhanced moisture layer may aid future convection (e.g., Li et al. 2014; Schlemmer and Hohenegger 2014). As drops reach larger sizes through collision-coalescence (e.g., Baker et al. 2009) and their corresponding size-dependent fall velocities increase, drops can reach the ground with only partial evaporation.

The convective organization established by surface-based precipitation-induced cold pools differs fundamentally from the larger-scale convective self-aggregation discussed elsewhere in this volume (e.g., Holloway et al. 2017; Wing et al. 2017). In convective self-aggregation, radiative subsidence produces an expansive ( $> 1000$  km), convectively suppressed, dry region (a “dry pool”) that is growing in time, neighboring a moist, deep convective region. Although an analogy between the radiative dry pool and evaporation-driven cold pools is often made, there are important differences. In the simulation shown in Fig. 1a and b, the driest precipitable water (PW) percentile corresponds to the “dry pool,” and the moistest PW percentile to the convective regime capable of supporting cold pools. A dry region is seen to form and expand, confining the deep convection to the remaining moist area. Convective self-aggregation is most clearly exhibited within radiative-convective equilibrium models of tropical convection. Observations in nature of convective self-aggregation remain elusive (Holloway et al. 2017) and difficult to attribute to specific feedbacks, but one study examining observed aggregation depicts properties similar to modeled self-aggregation, including large-scale drying (Tobin et al. 2012).

Convective organization leads to an enhancement of moisture gradients, as moist regions become moister and dry regions become drier, evident in Fig. 1. The mesoscale convective cold pools within the convectively self-aggregated regions can act to oppose the aggregation, by transporting water vapor from moist to dry areas, reflecting the divergence resulting from strong downdrafts in the subcloud layer in the model moist cold pools (Fig. 1e). In nature, the most dramatic visual example of this is arguably cold-pool-containing squall lines emanating from the African monsoon into the Sahara desert (e.g., Flamant et al. 2009; Trzeciak et al. 2017). Over the tropical ocean, cold pools within

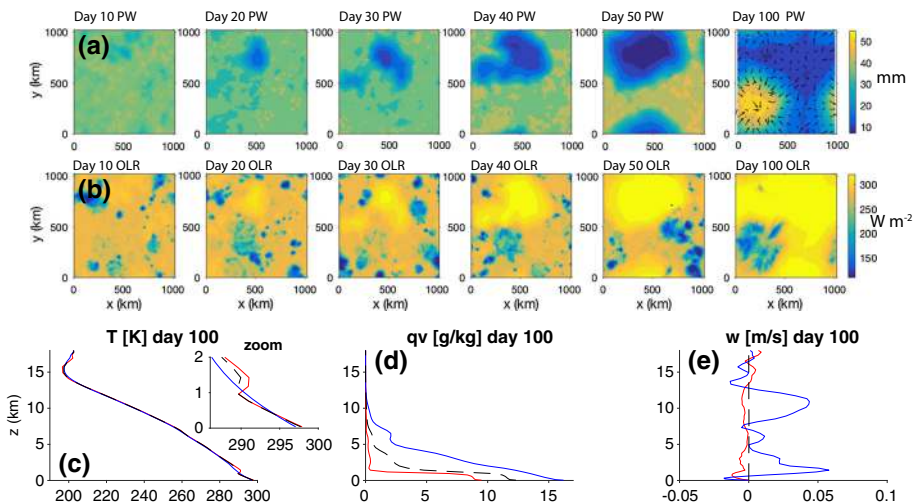


**Fig. 1** Time evolution showing days 10, 20, 30, 40, 50 and 100 of **a** precipitable water  $PW(t)$  and **b** outgoing longwave radiation  $OLR(t)$  in a cloud-resolving model called System for Atmospheric Model (SAM) with doubly periodic boundary conditions and without large-scale forcing. The last panel of PW (day 100) also shows the low-level winds, which are seen to converge into the moist aggregate. Vertical profiles of **c** temperature, **d** water vapor and **e** vertical velocities in the radiatively subsiding dry pool, identified by  $PW \leq 20$ th percentile, and in the precipitation-induced cold pools, identified by the near-surface (first atmospheric level  $z = 37$  m) temperature  $T_{air} \leq 20$ th percentile, and precipitation  $> 0$  at the end of the simulation. An inset in the first 2 km added to **c** to indicate the inversion in the dry pool at the top of the subcloud layer

simulated squall lines help broaden the precipitating intertropical convergence zone poleward (Nolan et al. 2016). Precipitatively-generated cold pools also counteract convective self-aggregation through suppression of local convection by divergence of the near-surface air (Fig. 1e) (Jeevanjee and Romps 2013; Muller and Bony 2015). In theory, such mesoscale subsidence within a precipitation cold pool could morph into a new, larger radiatively induced “dry pool,” although this model behavior has not yet been witnessed, to our knowledge (see also Held et al. 1993; Muller and Held 2012).

Cold pools act to disperse convection. Atmospheric cold pools over oceans are receiving attention for their ability to reorganize the mesoscale cloud distributions and potentially facilitate the transitions from high- to low-albedo shallow cloud cover. In the Tropics, the expansion of the spatial and height distribution of convection by cold pools may facilitate transitions from shallow to deep convective regimes, and therefore the eastward propagation of the Madden–Julian oscillation (MJO) into moistening environments (Rowe and Houze 2015; Feng et al. 2015; Ruppert and Johnson 2015; Schlemmer and Hohenegger 2016; Hannah et al. 2016; Ciesielski et al. 2017).

These foci on cold pool impacts justify the timeliness of a survey of cold pool characteristics and processes in different convective regimes. New observational capabilities and strategies were employed during the Rain in Cumulus over Ocean campaign (RICO; Rauber et al. 2007) and Dynamics of the MJO campaign (DYNAMO; Yoneyama et al. 2013) and will be during the upcoming Elucidating the role of clouds-circulation coupling in climate campaign (EUREC<sup>4</sup>A; Bony et al. 2017). These advance early observational studies stymied by imprecise data collocation and measurement misunderstanding (e.g., Warner et al. 1979; LeMone 1980) that had difficulty perceiving the larger-scale mesoscale organization. Measurements either came from one point, e.g., a ship (Addis et al. 1984; Young et al. 1995; Saxen and Rutledge 1998) or from aircraft (e.g., Zipser 1977; Kingsmill and Houze 1999), convoluting space and time. Modeling capabilities are improving also, either in their spatial grid spacing (Romps and Jeevanjee 2016; Grant and van den Heever 2016) or domain size (Schlemmer and Hohenegger 2014, 2016), and at times both (Seifert and Heus 2013; Vogel et al. 2016). The recent years have also seen advances in the formulation of cold pool parameterizations (e.g., Qian et al. 1998; Rozbicki et al. 1999; Rio et al. 2009, 2013; Grandpeix and Lafore 2010; Grandpeix et al. 2010; Hohenegger and Bretherton 2011; Del Genio et al. 2015; Pantillon et al. 2015) and their coupling with convective schemes. These provide an avenue for rectifying a model diurnal cycle that is too closely linked to the solar cycle in models (Rio et al. 2009; Grandpeix et al. 2010; Schlemmer and Hohenegger 2014).

The focus in this survey is over ocean in the subtropical and tropical latitudes. Cold pools are extremely important over land for initiating convection, where their depth and gust fronts are often substantial (e.g., Bryan and Parker 2010), surface sensible fluxes are significant and aerosol effects are more pronounced (e.g., Grant and van den Heever 2015, 2016; Schlemmer and Hohenegger 2016). Cold pools are also important for squall lines and tornadogenesis (e.g., Markowski and Richardson 2014). The omission of land-based cold pools is merely to keep the scope of this particular survey tractable. The focus on the oceanic regions equatorward of  $\sim 30^\circ\text{N}$  also emphasizes near-surface latent cooling induced by the partial evaporation of the liquid phase, as opposed to cooling by ice melting or sublimation. Cold pool behavior and significance vary with the depth of the originating convection, its degree of organization and relationship to the large-scale environment (trade wind vs. equatorial). This is reflected in the structure of the survey, which begins with shallow convection and moves toward deeper convection. The

subtropical and trade wind regions are defined by climatologically steady winds imposing a background wind shear, extending to Barbados in the examples provided and cited literature. The tropical ocean examples and cited literature are primarily near-equatorial, where wind shear can be ignored at times, and convection is readily able to span the full free troposphere.

## 2 Cold Pools from Boundary Layers not Exceeding 2 km Altitude

The strong inversion capping subtropical stratocumulus clouds maintains cloud top heights at  $\sim 1.5$  km or less (Zuidema et al. 2009), yet drizzle is ubiquitous (Leon et al. 2008). Some of the precipitating clouds occupying slightly deeper boundary layers (e.g., Mechem et al. 2012) are capable of downdrafting air that can reach the surface and develop cold pools (e.g., Fig. 2), also documented in Savic-Jovcic and Stevens (2008) and Wood et al. (2011). Aircraft measurements within stratocumulus cold pools indicate that near the surface the equivalent potential temperature ( $\theta_e$ ) tends to increase, rather than maintain a constant value or decrease (Zanten and Stevens 2005; Savic-Jovcic and Stevens 2008; Terai and Wood 2013).<sup>1</sup> The increase in  $\theta_e$  is attributed to an accumulation of the surface fluxes underneath a cold pool capping stratification. Cold pool depth is difficult to observe. Inferences made from pressure increases suggest altitudes of  $\sim 300$  m (Terai and Wood 2013, and references therein). Further aloft, evaporation at constant moist static energy still brings air closer to saturation, increasing its susceptibility to convection. Wind speed convergence of the convectively favorable air near the cold pool edges helps perpetuate open-celled organization (Feingold et al. 2010), ventilating the accumulated surface fluxes and mixing air through the boundary layer. Thus, alterations to both the thermodynamic vertical structure and surface dynamics provide mechanisms by which cold pools can contribute to the longevity of precipitation within stratocumulus regions, in both closed- and open-celled organizations. Precipitation is most pronounced pre-dawn (e.g., Burleyson et al. 2013), suggesting that cold pools are also most effective at night.

Radar observations indicate that the speed of advection of cold pools is similar to that of the cloud layer (Wilbanks et al. 2015). This suggests that cold pools are better thought of as tracers or artifacts of stratocumulus precipitation as opposed to drivers. This is also concluded from simulations relying on fixed cloud droplet numbers (Zhou et al. 2017) and is consistent with simulations showing little influence on cloud organization from the inhomogeneization of surface fluxes by cold pools (Kazil et al. 2014). Precipitation is necessary for transitions from closed- to open-cell stratocumulus cloud organizations (e.g., Savic-Jovcic and Stevens 2008; Xue et al. 2008; Wang and Feingold 2009; Feingold et al. 2010; Wood et al. 2011), thereby implicating cold pools in mesoscale organization transitions, but only indirectly. Aerosol number concentrations must also deplete sufficiently for open-celled or cumuli organization to form (Wood et al. 2011; Zhou et al. 2017; Yamaguchi et al. 2015). That said, aerosol budgets are unlikely to be influenced by cold pools per se, as the wind increases at cold pool fronts are shortlived (Terai and Wood 2013), except perhaps in strongly aerosol-depleted conditions (Kazil et al. 2014). It is also noteworthy that, while an important motivation for studying shallow mesoscale transitions is their influence on cloud fraction and the planetary albedo, a clear relationship between

<sup>1</sup> A notable contradictory observation, of stratocumulus clouds reaching only 1.5 km yet able to transport drier air downward from aloft, is documented in Jensen et al. (2000); the conditions explaining the difference remain underexplored.



**Fig. 2** September 14, 2016 MODIS *Terra* 10:30 am LT visible image near Ascension Island ( $14^{\circ}\text{W}$ ,  $8^{\circ}\text{S}$ ), located in the upper-left-hand corner of the image. The highest cloud tops reach 1.7 km, as detected by a cloud radar located on Ascension as part of the DOE Layered Atlantic Smoke Interactions with Clouds campaign (Zuidema et al. 2016). Radiosonde winds indicate west-northwestward boundary layer flow (yellow vector)

precipitation and cloud cover is not apparent in Fig. 2, as the precipitation feeds an upper stratiform layer below the trade wind inversion. Nuijens et al. (2015) clarify that it is this cloud layer, rather than a lower cloud layer at the lifting condensation level, that is most variable.

As air advects from the stratocumulus regions to warmer sea surface temperatures, the altitude of the trade wind capping inversion rises only slowly (Schubert 1995), but the weakening temperature inversion does begin to permit deeper convection. Early experiments studying the suppressed trade wind/tropical convective environment, namely the Atlantic Trade wind Experiment (ATEX; Augstein et al. 1973) and the Barbados Oceanographic and Meteorological Experiment (BOMEX; Nitta and Esbensen 1974), estimated the fractional area occupied by actively ascending cumuli to be a negligible 0.02 (Augstein et al. 1973). The prevailing cloud organization was isolated cumuli or cloud lines aligned with the mean wind that precipitated very little if at all (LeMone and Pennell 1976; Nair et al. 1998), suggesting that cold pools can likely be ignored for this environment (e.g., Albrecht 1993; Siebesma et al. 2003). This supported a paradigm begun with Riehl et al. (1951) in which precipitation within the boundary layer does not change the moist static energy, but rather the cooling introduced by evaporating rain is energetically balanced by an increase in moisture.

### 3 Cold Pools from Convection Reaching the Mid-Troposphere

The diffusing trade wind inversion strength does allow some deeper clouds to develop, however, and along with them, cold pools. Larger drop sizes, encouraged by a stronger collision-coalescence process, allow precipitation to return approximately one-third of the surface evaporation to the ocean in the trade wind cumulus region (Snodgrass et al. 2009). Visible in Figs. 3 and 4 are examples of isolated convection in the northeast Atlantic trade winds able to reach 4 km coexisting with cloud lines lacking precipitation. These images are representative of the northeast Atlantic (Zuidema et al. 2012; Nuijens et al. 2017). The



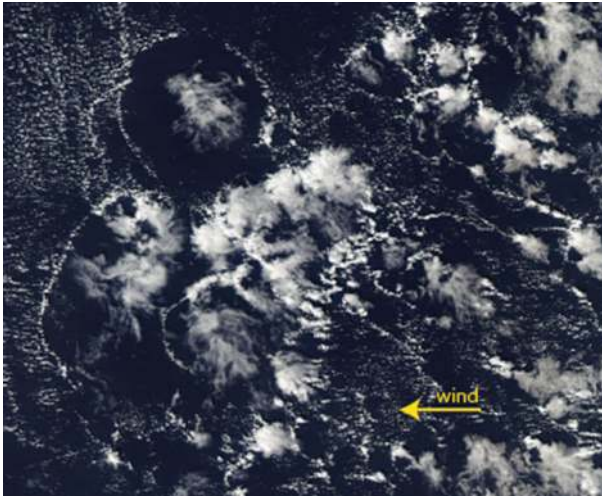


**Fig. 3** December 19, 2013, MODIS *Aqua* 13:30 pm LT visible image, east of Barbados (46.5–50°W, 17.5–20°N) coincident with the Next-generation Airborne Remote Sensing for Validation (NARVAL) aircraft campaign (Stevens et al. 2016, 2017). The wind is flowing from right to left. The two largest cold pools span approximately 100 km and are better defined on the downwind side, particularly the left side of the image. The higher cloud tops within the cold pool centers reach approximately 4 km



**Fig. 4** Aircraft view of a cold pool taken on August 25, 2016, southeast of Barbados. Noteworthy are the cloud lines to the left of the image, with the nearby cold pool convection organized in a circle, a portion of which is oriented perpendicular to the cloud lines in the left-hand side. Isolated convection reaching a higher altitude is detraining, most likely into a layer of increased stability

deeper clouds spawn downdrafts capable of bringing down air that is drier than the near-surface air, contributing to a lowering of the equivalent potential temperature (Zuidema et al. 2012). The presence of less convectively favorable air near the surface, spreading out as a density current, explains an organization of mesoscale cloud arcs circumscribing mostly cloud-free regions. The small areal coverage of the deeper clouds can thus alter a much larger area of near-surface air. More quantitatively, the satellite-derived cloud fraction producing rain rates exceeding  $1 \text{ mm h}^{-1}$  is a mere 0.02 for wintertime Caribbean cumuli (Snodgrass et al. 2009), over an area of approximately  $\sim 10^4 \text{ km}^2$  scanned by a

precipitation radar, also consistent with estimates from large-eddy-scale simulations (Neggers et al. 2002). The diurnal cycle is weak (Snodgrass et al. 2009).

A further notable feature of Figs. 3 and 4 is their siting at approximately 10°N of the intertropical convergence zone (ITCZ), after a multi-day equatorward advection of boundary layer air away from the stratocumulus regions. At what point along the journey shallow convection can deepen substantially remains underexplored. Space-based lidar suggests the northern hemisphere ocean basins are more conducive of 'deeper' shallow convection (Fig. 1 of Medeiros et al. 2010), perhaps because northern hemisphere surface parcels do not advect over cooler equatorial waters in their journey to the ITCZ. The environmental conditions supporting shallow convection that can become deep enough to support coherent downdrafts bringing down air of lower  $\theta_e$  from above the cloudy boundary layer is also not known and may depend on the history of the air parcel as well.

Liquid-only clouds reaching 4 km produce cold pools that are very similar to those produced by tropical deep convection extending throughout the depth of the troposphere, shown next.

### 4 Cold Pools from Deep Tropical Convection

The mean properties of ~ 300 cold pools composited from conventional surface meteorological datasets from Gan Island (0.6°S, 73.1°E) and the Research Vessel *Roger Revelle* located ~ 700 km to the east, at 80.5°E are shown in Fig. 5. A cold pool is identified through a temperature drop of 0.5 K, applied to a 5-min time series that has been smoothed using a Haar wavelet filter, combined with the requirement of no rain within the hour prior. The temperature drops are normalized to their mean time span of 20 min. The cold pool

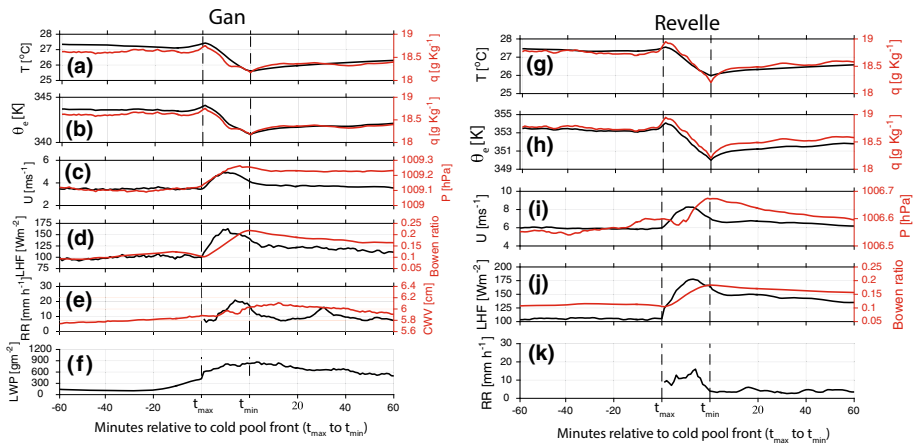


**Fig. 5** Cold pool composite based on 193 cold pools at Gan island (a–f) and 103 at the *Revelle* (g–k) between October 6, 2011 to December 31, 2011, from one prior to 1 h past the cold pool frontal passage. The cold pool front is defined through a temperature drop of 0.5 K applied to the 5-min time series smoothed using a Haar wavelet filter. The front is normalized to a 20-min time interval, corresponding to the mean frontal passage time. **a, g** Air temperature (black) and water vapor mixing ratio (red); **b, h** water vapor mixing ratio (red) and equivalent potential temperature (black); **c, i** surface wind speed (black) and surface pressure (red); **d, j** latent heat fluxes (LHF, black) and the Bowen ratio (surface heat fluxes/latent heat fluxes; red); **e, k** rain rate (black) and column water vapor (red, **e**) only; **f** liquid water path



sample is drawn from the full tropical convective spectrum. The composite-mean includes a near-surface drying of  $\sim 1 \text{ g kg}^{-1}$  and decrease in the equivalent potential temperature of 2 K. The mean wind speed increases by  $\sim 2 \text{ m s}^{-1}$ , but only for 15–30 min. The pressure increase corresponds to a mean cold pool depth of approximately 300 m, is that stronger temperature drops are accompanied by stronger decreases in the water vapor mixing ratio (and  $\theta_e$ ), indicating either higher origin heights for the downdrafts or more coherent structures less modified by environmental mixing (de Szoeke et al. 2017). The mean near-surface relative humidity of the cold pools indicate subsaturation (not shown), suggesting the downdrafts rarely if ever maintain saturation, despite being initially saturated. All of these traits are shared with cold pools in the northeast Atlantic trade wind regime (Zuidema et al. 2012).

Cold pools are much more likely to occur underneath obscuring cirrus shields (e.g., de Szoeke et al. 2017), but one example of a tropical cold pool visible from space is shown in Figs. 6 and 7, coinciding with the DYNAMO field campaign (Yoneyama et al. 2013). A vertically pointing cloud radar and meteorological station operated within the range of a scanning precipitation radar, with a range-height indicator scan dedicated to the precipitation radar azimuth encompassing the cloud radar (Feng et al. 2014), allowing a precise collocation of cold pool convective features with its surface features. The cold pool spanning  $\sim 120 \text{ km}$  is outlined on the 0615 UTC image, reaching the surface site at approximately 0915 UTC, where the vertically pointing radar reveals a cloud depth of 12 km in places lacking wind shear. The visible image shows other cold pools that are less obvious in the radar image. The surface meteorological time series shows a water vapor path increasing from 5.1 to 5.6 cm prior to the cold pool, whose edge has a temperature drop of  $\sim 5 \text{ K}$ , a more quickly recovering drop in the vapor mixing ratio, and a short, almost unidentifiable, wind speed increase. The relative humidity at altitudes above 5 km was  $\leq 50\%$  (not shown).

Stratiform precipitation occurring later in the day prevented recovery of the near-surface temperature and maintained a near-surface relative humidity of 85–90%. Earlier observational studies focused on longer-lasting cold pools also selected from mesoscale systems with stratiform precipitation (e.g., Young et al. 1995), and longer-lasting surface fluxes changes are documented (Saxen and Rutledge 1998). For these, the altered surface fluxes, with their higher Bowen ratio, may be enough to influence the mean. This is one difference from cold pools in the trade wind regime. Deep tropical convection with stratiform precipitation can also sustain mesoscale downdrafts of warmer air. Early aircraft measurements concluded mesoscale downdrafts are too warm to reach the surface (Zipser 1977), but this is contradicted by Kilpatrick and Xie (2015), who relied on satellite scatterometer data combined with surface buoys.

Other influences on tropical cold pool characteristics, besides the level of mesoscale organization, include the atmospheric moisture distribution and the amount of mixing with environmental air during the downdraft. Since tropical deep convection easily attains cloud top heights of 8 km and upwards (Fig. 8), the downdraft air can in theory originate from a higher altitude. The modification of near-surface air properties is indeed more pronounced when the cloud top heights of the parent convection are higher (Fig. 8). Most studies point to an origin altitude for the downdraft air of 2 km or less, however (Betts 1976; Betts and Dias 1979; Torri and Kuang 2016a; de Szoeke et al. 2017; Schiro and Neelin 2017). That higher clouds are associated with stronger cold pools may reflect a correlation between downdraft width and clouds that are wider as a result of organization, discouraging environmental dilution of the downdraft air (Schlemmer and Hohenegger 2014; Schiro and

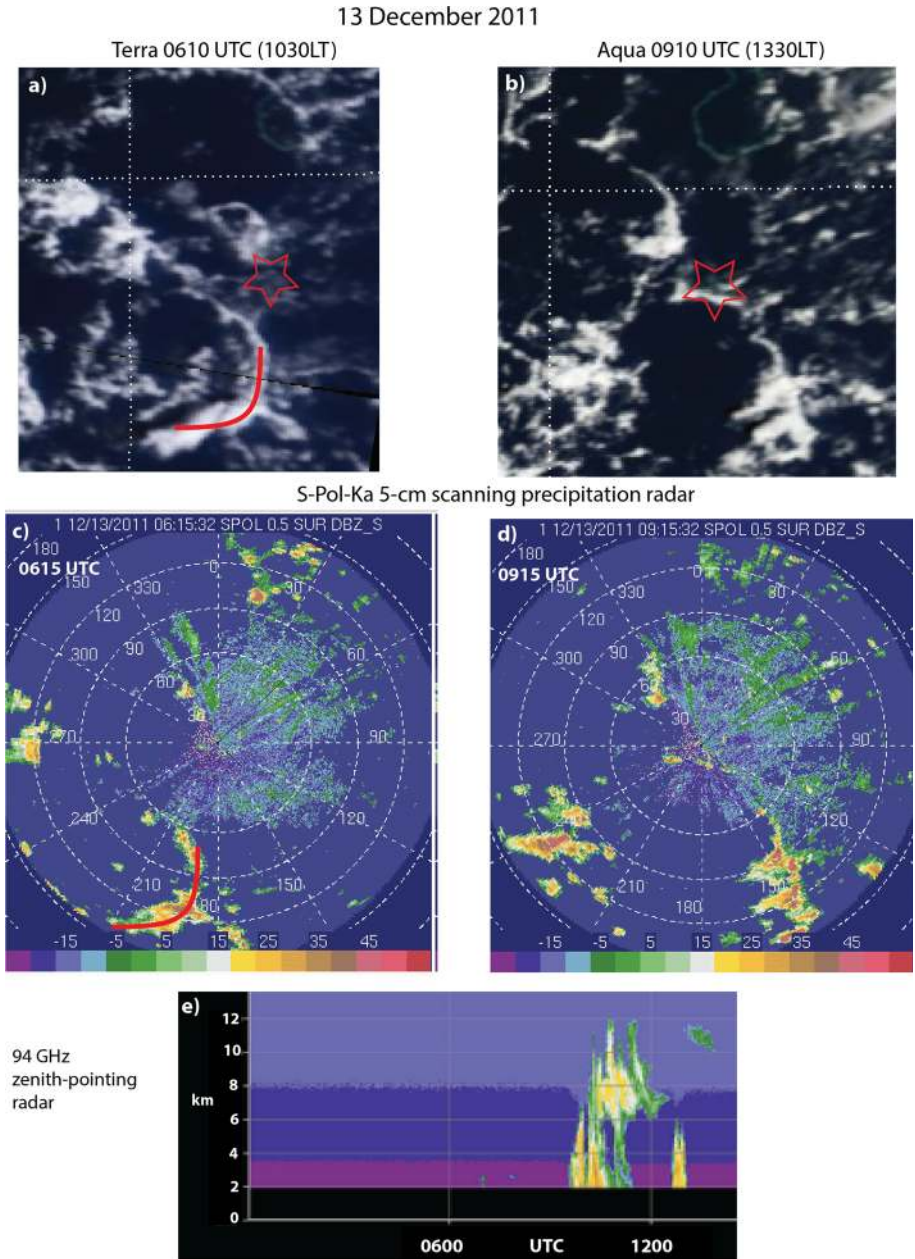


**Fig. 6** **a** *Terra* and **b** *Aqua* December 13, 2011 MODIS visible satellite imagery of cold pool mesoscale organization in the equatorial Indian Ocean with **c**, **d** near-in-time 5-cm scanning precipitation radar surveillance scan imagery corresponding to **a**, **b**. **e** A 94-GHz vertically pointing radar located on Gan Island indicates the height of the corresponding convection. Red stars indicate Gan island ( $0.6^{\circ}\text{S}$ ,  $73.1^{\circ}\text{E}$ ). The red half-circles in panels **a**, **c** correspond to the cold pool arriving at Gan island  $\sim 3$  h later

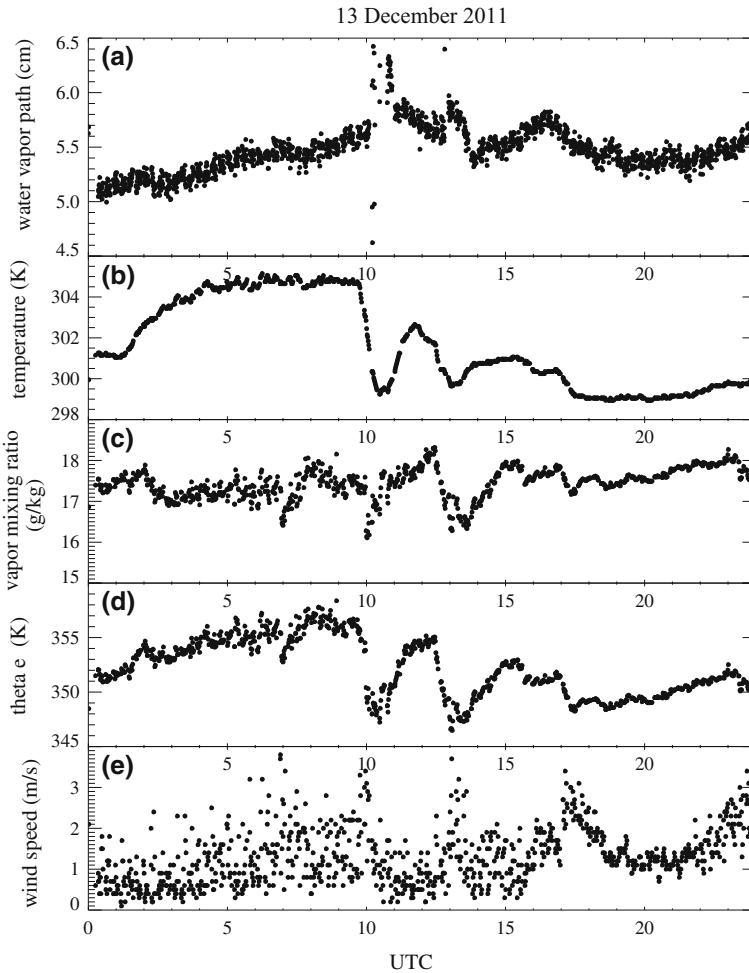


**Fig. 7** December 13, 2011 time series from a surface meteorological station and microwave radiometer on Gan Island of **a** water vapor path, **b** temperature, **c** water vapor mixing ratio, **d** equivalent potential temperature and **e** wind speed

Neelin 2017; Mapes et al. 2017). The low-altitude origin discounts contributions to the convective downdrafts (treated separately from stratiform precipitation) by the melting or sublimation of ice particles (Srivastava 1987).

Convection able to impinge upon relatively dry mid-tropospheres should in theory also produce stronger cold pools, by allowing more evaporation into the downdraft while simultaneously transporting drier air of lower  $\theta_e$  to the surface (e.g., Chen et al. 2016). Many examples of drier atmospheres coexisting with more isolated convection are documented within shallow-to-deep transition studies (Feng et al. 2014; Ruppert and Johnson 2015), as well as with linearly organized convection such as squall lines (Takemi and Satomura 2000; Mapes et al. 2017; Schiro and Neelin 2017). A correspondence between stronger cold pools and drier mid-tropospheres has not yet been robustly identified in observations, but is consistent with published emphases (see also Takemi et al. 2004). One

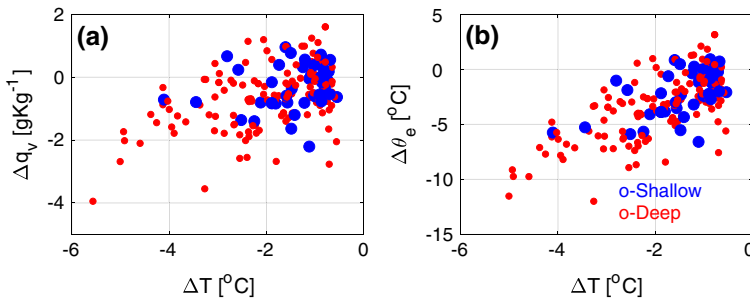


**Fig. 8** Changes in **a** water vapor mixing ratio and **b** equivalent potential temperature low as a function of cloud top height ( $< 4$  km in blue,  $> 4$  km in red), from a surface meteorological station at Gan island ( $0.6^{\circ}\text{S}$  and  $73.2^{\circ}\text{W}$ ), in the equatorial Indian ocean. Cloud top heights inferred from a 35-GHz-band zenith-pointing radar. The initial temperature and moisture values correspond to the 1-min smoothed value before the cold pool temperature drop, and the minimum temperature thereafter represents the end of the cold pool frontal passage, with a criterion of a temperature drop of at least 0.5 K applied

important compensation is the condensate loading within the downdrafts, as more condensate will decrease the surface parcel buoyancy (James and Markowski 2010; Torri and Kuang 2016a).

Tropical cold pools are more frequent during times of lower outgoing longwave radiation, reflecting more organized deep convection with larger cloud covers, cooler sea surface temperatures (SSTs), and cooler near-surface layers that are closer to saturation (de Szoeke et al. 2017), and more fully saturated atmospheres. The number of observed cold pools only varies weakly with time of day (de Szoeke et al. 2017), though satellite measurements suggest mesoscale downdrafts able to reach the surface occur 8–12 h after the peak rainfall (Kilpatrick and Xie 2015). The boundary layer is cooled and moistened over a large area by the evaporation of stratiform precipitation, reducing the buoyancy of individual surface parcels. Nevertheless, cold pools and the surface-originating convection they reflect clearly do occur (de Szoeke et al. 2017), perhaps more than originally thought at the time of Houze and Betts (1981). This is also evident in space-based cloud radar observations of cumulus congestus/cumulonimbus occurring underneath upper-level stratiform cloud (e.g., Riley et al. 2011). The moisture distribution is influenced more by layer-lifting and less by surface-based buoyancy (see, e.g., in this issue, Mapes et al. (2017), dating back to at least Houze and Betts (1981), so that it cannot be argued that cold pools are important for redistributing moisture.

A connection between deep convective cold pools and those in the trade wind regions may then be their relationship to the column water vapor path. In the trade wind regions, column water vapor paths of 4.5–5.0 cm correspond to moister free tropospheres capable of supporting deeper convection and more cold pools (Zuidema et al. 2012). The DYNAMO water vapor path frequency distribution contains a plateau at 5.8–5.9 cm, and a mean of 5.1 cm (Zhang et al. 2017), suggesting the slightly drier conditions in which cold pools can be more influential are close in value to those for the trade wind regions. This is consistent with the subcloud moisture field remaining critical for convective initiation (Kingsmill and Houze 1999; Seifert and Heus 2013), particularly at cloud base level (Takemi and Satomura 2000), as well as anomalous moisture in the lower free troposphere (Sherwood et al. 2010), since column water vapor paths between 4.5 and 5.5 cm allow drier mid-tropospheres to coexist with deep, moist lower free tropospheres (Zhang et al. 2017).

One long-standing question in the Tropics, to which cold pools are relevant, is what maintains its boundary layer. The powerful Arakawa and Schubert (1974) parameterization assumes a quasi-equilibrium moisture closure in which surface moisture fluxes are balanced by the clear-sky entrainment of air drier than the saturation surface vapor mixing ratio. This is questioned within Raymond (1995), which concluded that surface fluxes must be balanced by convective downdrafts rather than clear-sky entrainment, because downdrafts provide a larger reduction in near surface  $\theta_e$ . In the more comprehensive observational assessment of de Szoeke et al. (2017) based on DYNAMO soundings, downdrafts contribute to 20–30% of the boundary layer moisture and temperature budget, on days with diminished sea surface temperature (SST), and less otherwise. This suggests the effects of downdrafts are secondary, if not negligible, to those from clear-air entrainment through the boundary layer top, on the boundary layer  $\theta_e$ . Thayer-Calder and Randall (2015) in an updated simulation also conclude clear-air entrainment predominantly balances surface evaporation. Torri and Kuang (2016a) also find a small contribution from convective downdrafts to the net flux of moist static energy into the boundary layer, and a much larger contribution from turbulent mixing across the boundary layer top, using a Lagrangian particle tracking analysis. These recent, independent studies all indicate a secondary role for downdrafts on the large-scale boundary layer moist static energy budget.

## 5 Remaining Questions

This survey motivates two remaining, intertwined questions.

### 5.1 The Relationship of Trade Wind Cold Pools to Cloud Cover

An outstanding question with shallow convection remains the still poorly known relationship between convection and cloud cover in the trade wind region, where the cloud cover is important for the planetary albedo. Modeling simulations, despite their many advances (e.g., Seifert and Heus 2013), remain inconclusive (van Zanten et al. 2011), to a substantial degree because many microphysical parameterizations are not optimal for trade wind cumuli representations (Li et al. 2015). While the cold pool itself discourages further surface-based convection, detraining elsewhere in the troposphere increases cloud cover. In Fig. 4, the deeper convection is detraining at a higher altitude, affecting the overall cloud cover, arguably also visible in Fig. 3. Such detraining can occur into layers of increased stability, and although the altitude of the higher stable layer is not clear in Fig. 2, the 0 °C level, which occurs at  $\sim 500$  hPa, is enriched with such layers (Zuidema 1998; Stevens et al. 2017).

This undertaking also means critically assessing microphysical parameterizations and their interaction with representations of environmental mixing. Experimentation with two popular microphysical schemes has revealed significant differences in cloud fraction ensuing from cold pools that are similarly simulated (Li et al. 2015), and relevant observations should also be acquired to assess results from arguably better-suited schemes (Seifert and Heus 2013). The sensitivity of the convective downdraft to condensate loading and mixing above the boundary layer is also important. In addition, this means further evaluating the effects of low- and high-wind shear, as wind shear can interact dynamically with the convective structure (Li et al. 2014). Related to all these questions is also the timescale of the boundary layer recovery within a cold pool, and how often cold pools are

able to fully recover before being impinged upon by a subsequent cold pool; observations suggest cold pools occur in clumps (e.g., Fig. 2). If so, and embedded in larger-scale moisture envelopes, those in tandem can alter the atmospheric longwave radiative cooling on longer time and larger spatial scales than of just an individual cold pool.

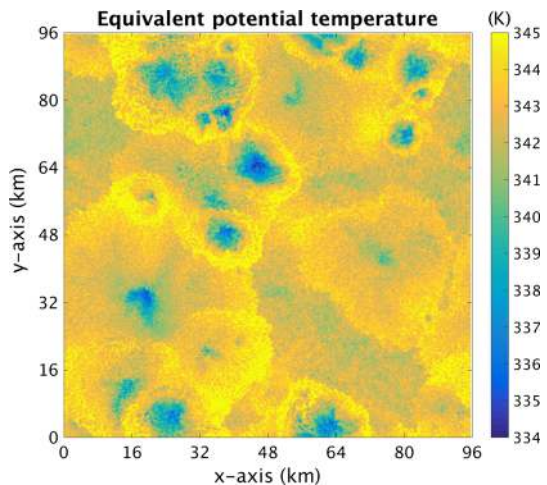
As computational capabilities continue to improve, the trade-off between spatial grid spacing and domain size in the modeling of cold pools can be expected to diminish. The enabled sophisticated examinations of cold pools with their larger-scale environment include examining the relative importance of colliding cold pools as opposed to single pools. The further development of tracking algorithms (Torri et al. 2015; Feng et al. 2015; Böing 2016; Drager and van den Heever 2017) within such more complex simulations will allow for a better understanding of collisions and their impact of the cold pool life cycle. Such efforts will also further parameterization development.

## 5.2 Thermodynamic Secondary Initiation Processes

Models, through their ability to capture the full four-dimensional fields (Fig. 9), highlight an important distinction between dynamical and thermodynamical influences on secondary convection. Early ideas for triggering new convection focused on dynamics, in which the cold density currents interacted with the prevailing near-surface wind shear to encourage upright updrafts favorable for convection (Rotunno et al. 1988). The trade wind regions in particular experience steady winds, with a maximum wind speed at cloud base decreasing both above and below. Dynamical forcing of boundary layer air is stronger when the cold pool gust front is aligned with the mean wind at the downwind side of a trade wind region cold pool, and the vorticity interactions help explain the more pronounced convection on the downwind side of a cold pool (e.g., in Figs. 3 and 4, further explored in Li et al. 2014). Stronger dynamical forcing is also related to higher downdraft heights in Jeevanjee and Romps (2015).

In tropical oceanic regions lacking rotation and strong wind shear (Fig. 5), a separate paradigm emphasizing the role of water vapor in initiating new convection has also been influential (Tompkins 2001). In the study of Tompkins (2001), cloud-resolving simulations using a doubly periodic domain of 90 km, at a horizontal grid spacing of 350 m, and with

**Fig. 9** A snapshot of the near-surface equivalent potential temperature distribution from Torri and Kuang (2016b)





no imposed mean wind vertical structure, accumulate water vapor within the full outer one-third of the cold pool, by  $0.25 \text{ g kg}^{-1}$  in the mean. The moistening remained inside the gust front edge. The anomalous moisture was attributed to the evaporation of precipitation into temperature-recovered air before the downdraft of air from a higher-altitude source could reach the surface, and a straightforward calculation of how much rain could evaporate into the subcloud layer is consistent with the  $0.25 \text{ g kg}^{-1}$  increase evident in the composite mean (Langhans and Romps 2015). In this way, rain evaporation not only moistens the air, but it also raises the air's  $\theta_e$  (which is otherwise conserved with phase changes), creating a positive feedback in triggering further convection. Surface fluxes (and winds) were discounted because these would be diminishing at the cold pool edge, as also evident in the observational composite (Fig. 5).

More recent modeling experimentation with 'single-bubble' convection further emphasizes the existence and importance of enhanced near-surface moisture resulting from the parent convection, but attributes the source of the moisture primarily to surface fluxes (Langhans and Romps 2015; Romps and Jeevanjee 2016). Rain evaporation nevertheless remains important by contributing the anomalous moisture capable of reaching the cloud base (Torri and Kuang 2016b). Similar to Tompkins (2001), the moisture in both these studies remains inside the cold pool edge.

The observational composites in Fig. 5 do not show widespread enhancements of water vapor mixing ratio  $q_v$  interior to the cold pool. A slight observed enhancement in  $q_v$ , of  $0.25 \text{ g kg}^{-1}$ , instead, appears at the cold pool edge, and prior to the wind increase. The increase in temperature of  $\sim 0.1 \text{ K}$  could conceivably reflect how the temperature drop is identified, but that would not explain the  $q_v$  increase. Such prior moisture increases were also noted in the tethered balloon measurements analyzed within Addis et al. (1984) and associated with upward vertical velocities. Their presence prior to the wind speed increases points to a convergence of the surface wind, and with it, moisture. The slight temperature increase could also be explained in this way.

The question then arises why models produce water vapor rings (e.g., Langhans and Romps 2015). Model cold pools can be composited similarly to observations, using time series at model grid points in the lowest model layer. Three examples, all based on the System for Atmospheric Modeling (SAM; Khairoutdinov and Randall 2006), are shown in Figs. 10 and 11. The composites shown in Fig. 10 incorporate large-scale forcings driven DYNAMO observations (Wang et al. 2015) and utilize a one-km horizontal grid spacing. Figure 11 show composites based on the Torri and Kuang (2016b) simulations, with an additional simulation performed using a smaller grid spacing (80 vs. 250 m), but otherwise identical. All three simulations lack wind shear.

Similarly to the Tompkins (2001) composites, a water vapor mixing ratio increase is seen to occur within the cold pool frontal edge, before a decrease after the frontal passage. This occurs within all three simulations. The simulations in Fig. 11 do place the water vapor increase closer to the front, but are themselves not sensitive to the horizontal grid spacing. The model  $q_v$  increases exceed those observed, also evident in Fig. 3 of Feng et al. (2015). These comparisons suggest models may overproduce water vapor rings. Postulated explanations can include an under-entrainment of drier air into the gust front edge or excessive evaporation, reflecting turbulent mixing and microphysical processes that are difficult to represent accurately, or a surface flux-wind feedback that is too strong. In Fig. 11, the simulation with the smaller grid spacing produces surface fluxes that are slightly lower than in the other simulation ( $102.7$  vs.  $100.6 \text{ W m}^{-2}$  for the latent heat fluxes, and  $9.58$  vs.  $9.48 \text{ W m}^{-2}$  for the sensible heat fluxes), and may be due to different

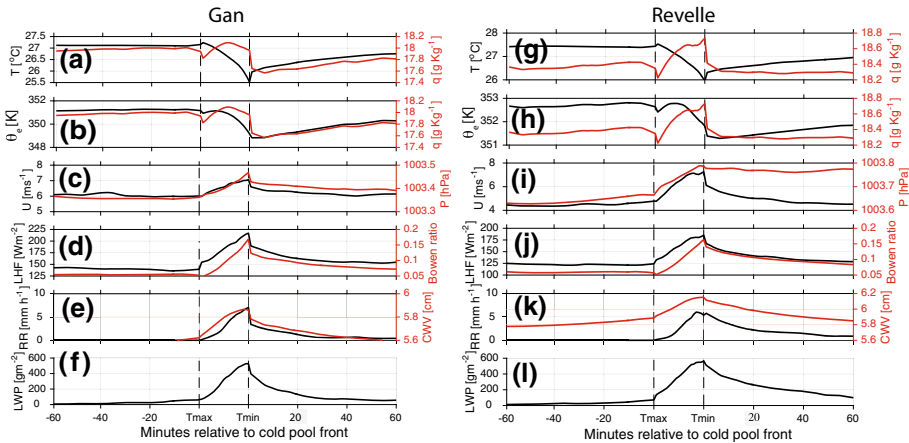


**Fig. 10** Composites of **a, g**: air temperature (black) and water vapor mixing ratio (red); **b, h** water vapor mixing ratio (red) and equivalent potential temperature (black); **c, i** surface wind speed (black) and surface pressure (red); **d, j** latent heat fluxes (LHF, black) and the Bowen ratio (surface to latent heat fluxes; red); **e, k** rain rate (black) and column water vapor (red, **e**) only; **f, l** liquid water path, based on SAM simulations. The left **a–f** panel applies to Gan island from two time periods combined, October 8–16 and December 18–25, 2011. The right **g–l** panel applies to *R/V Reville* simulations spanning October 2 to November 1, 2011. The doubly periodic simulations at a one-km horizontal grid spacing incorporate daily large-scale forcings developed for the DYNAMO time period from the campaign observations (Wang et al. 2015). 5-min model output was evaluated at 16 grid points within a 256 km by 256 km spatial domain

gust front velocities, while evaporation rates are slightly higher when the grid spacing is smaller. More work is required to confidently explain the differences beyond the scope of this current contribution, with this example primarily introduced to highlight the need for a benchmark dataset of both observations and model simulations.

In addition, model simulations of cold pools generally make trade-offs between domain size and grid spacing.<sup>2</sup> Studies that use larger domain sizes to represent cold pool mesoscale organization are more likely to attribute anomalous moisture sources for secondary convection outside of the cold pool (Li et al. 2014; Schlemmer and Hohenegger 2016). This is also consistent with the observed inhomogeneity of the secondary convection around the mesoscale arc (Figs. 2, 4) locations, where a dynamical lifting of a surface parcel is most able to access moisture, will be the most likely to see convection thrive (see also Torri et al. 2015). Further advantages of larger domains are the ability to capture colliding cold pools (e.g., Fig. 9), and, when incorporating the large-scale forcing at the boundary as opposed to using doubly periodic domains, the ability to capture cold pool asymmetries (Li et al. 2014, 2015). Wind shear aloft can modify the cloud's geometry, thus limiting cloud deepening (Zuidema et al. 2012; Li et al. 2014) but can also increase evaporation (Schlemmer and Hohenegger 2014), as well as allow the precipitation to fall outside of the main updraft core, and has bearing on the overall cloud fraction.

<sup>2</sup> For example, Roms and Jeevanjee (2016) use a horizontal grid spacing of 50 m and a vertical grid spacing as high as 10 m in the bottom 600 m of the computational domain. Grant and van den Heever (2016) imposed a 50-m grid spacing in the horizontal and 25 m in the vertical, within a two-dimensional cold pool. In contrast, Schlemmer and Hohenegger (2014) and Schlemmer and Hohenegger (2016) use a computational domain of  $256 \times 256 \text{ km}^2$  with a horizontal grid spacing of 250 m, and Li et al. (2014) and Li et al. (2015) use a large outer domain of  $972 \times 972 \text{ km}^2$  nesting an inner domain with a 100-m grid spacing. Seifert and Heus (2013) use a  $50 \times 50 \text{ km}^2$  domain with grid spacings of 25–100 m.

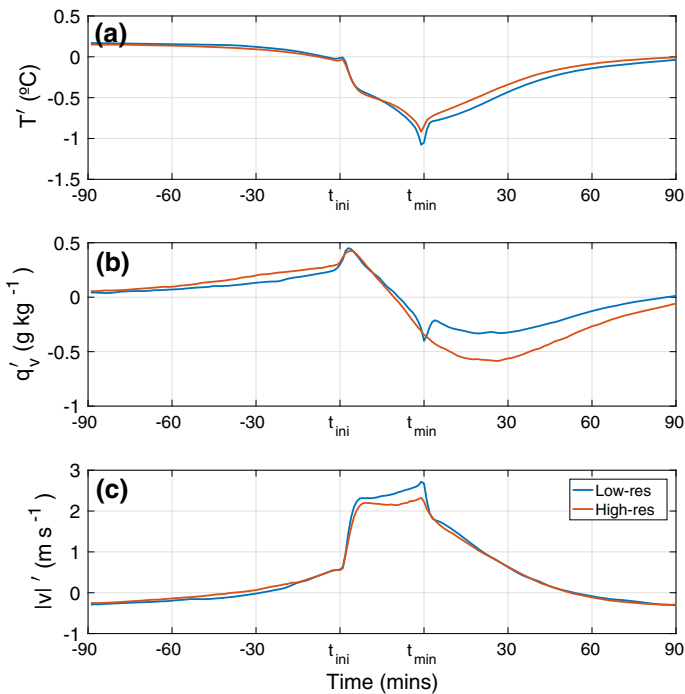


**Fig. 11** Composites of **a** temperature, **b** water vapor and **c** wind speed based on the Torri and Kuang (2016b) model simulations, at 250- and 80-m horizontal grid spacings (blue and red lines, respectively), shown as anomalies from a 2-h mean to control for model drift. Cold pool selection is based on a virtual temperature drop of 0.5 K within a 10-min time period at 10,000 random points within the 30-meter bottom layer ( $t_{ini}$ ). The history between  $t_{ini}$  and  $t_{min}$  interpolated to a fixed length, similar to Fig. 5. Domain size is 64 km by 64 km, with the model output saved every 30 min over 2.5 days

The dominating remaining observational challenge arguably remains the need to better resolve the four-dimensional humidity field. The idea that the updraft air feeding convection tends to have a high  $\theta_e$  (or equivalently, moist static energy) is not controversial, either observationally (Kingsmill and Houze 1999) or theoretically (Emanuel et al. 1994). Consensus about the source of the anomalous moisture and equivalent potential energy ( $\theta_e$ ) for the secondary convection that is triggered by cold pools has not yet been reached. The distribution of moisture near cloud base remains poorly known, along with the vertical structure of cold pools. This is unlikely to be solved soon via remote sensing (see, e.g., Mapes et al. 2017; Zhang et al. 2017), with what is possibly the best passive remote sensing technique, using spectral infrared (Blumberg et al. 2015) still primarily limited to clear skies. Differential absorption and Raman lidars can profile moisture (Kiemle et al. 2017) but are obstructed by cloud, although extrapolation from points nearby could provide insight, and in combination with Doppler wind lidar might be able to resolve moist updrafts. The measurement of the most important state variables can also be readily done as the standard package on a small research aircraft and now also on drones and unmanned aerial vehicles (e.g., <http://vandenheever.atmos.colostate.edu/vdhp/c3loud-ex/index.php>), or using small, light balloons as pseudo-Lagrangian drifters (<https://sites.psu.edu/pmarkowski/2017/06/07/markowski-and-richardson-fly-dozens-of-airborne-probes-into-three-severe-storms-in-oklahoma-and-kansas/>). This would shed further light on the relationship

of the thermodynamics to the cold pool dynamics as well as conceivably interaction with surface fluxes (Ross et al. 2004; Gentine et al. 2016; Grant and van den Heever 2016).

Future challenges also remain on the modeling front. For example, the influence of entrainment at the gust front remains an open question. Work has been done to determine the entrainment in gravity currents (see e.g., Hacker et al. 1996; Hallworth et al. 1996; Fragoso et al. 2013), but mostly in idealized scenarios, which raises questions on the applicability of these results to real-world cold pools. To address this question using numerical models is a challenging task as the simulations required for this purpose would have to be conducted in a large enough domain, and, at the same time, with a spatial grid spacing capable of properly representing turbulent mixing at the gust front (see Grant and van den Heever (2016) for such an attempt). Such efforts will also improve parameterizations of the boundary layer turbulent transports towards representing clear-air entrainment and up/downdrafts correctly (see also Tompkins and Semie 2017).

**Acknowledgements** PZ and AC gratefully acknowledge support from NOAA Climate Variability Program Grant NA13OAR4310157 and PZ from National Science Foundation grant AGS-132189. GT acknowledges support from DOE Award DE-SC0018120 and NSF Grant AGS-1649819. CM gratefully acknowledges CINES/GENCI and PRACE/TGCC in France for providing access and support to their computing platforms OCCIGEN and CURIE. The satellite imagery in Fig. 1 was acquired through the NASA Worldview website. We acknowledge use of DOE ARM Mobile Facility data within Fig. 5. We are thankful to Steve Krueger and Adam Kochanski for the SAM simulation data diagnosed in Fig. 10. We thank two anonymous reviewers for input that greatly improved the manuscript. This contribution is a result of the International Space Science Institute (ISSI) Workshop on “Shallow clouds, water vapor, circulation and climate sensitivity.”

**Open Access** This article is distributed under the terms of the Creative Commons Attribution 4.0 International License (<http://creativecommons.org/licenses/by/4.0/>), which permits unrestricted use, distribution, and reproduction in any medium, provided you give appropriate credit to the original author(s) and the source, provide a link to the Creative Commons license, and indicate if changes were made.

## References

- Addis RP, Garstang M, Emmitt GD (1984) Downdrafts from tropical oceanic cumuli. *Bound Layer Meteorol* 28:23–49
- Albrecht BA (1993) Effects of precipitation on the thermodynamic structure of the trade-wind boundary layer. *J Geophys Res* 98:7327–7337
- Arakawa A, Schubert W (1974) Interaction of a cumulus cloud ensemble with the large-scale environment, Part 1. *J Atmos Sci* 45:3188–3211
- Augstein E, Riehl H, Ostapoff F, Wagner V (1973) Mass and energy transports in an undisturbed Atlantic trade-wind flow. *Mon Weather Rev* 101:101–111
- Baker B, Mo Q, Lawson P, O'Connor D, Korolev A (2009) Drop size distributions and the lack of small drops in RICO rain shafts. *J Atmos Sci* 48:616–623
- Betts AK (1976) The thermodynamic transformation of the tropical subcloud layer by precipitation and downdrafts. *J Atmos Sci* 33:1008–1020
- Betts AK, Dias MFS (1979) Unsaturated downdraft thermodynamics in cumulonimbus. *J Atmos Sci* 36:1060–1067
- Blumberg W, Turner D, Lohnert U, Castleberry S (2015) Ground-based temperature and humidity profiling using spectral infrared and microwave observations. Part 2: actual retrieval performance in clear sky and cloudy conditions. *J Appl Meteorol Clim* 54:2305–2319. <https://doi.org/10.1175/JAMC-D-15-0005.1>
- Böing SJ (2016) An object-based model for convective cold pool dynamics. *Math Clim Weather Forecast*. <https://doi.org/10.1515/mcwf-2016-0003>.

- Bony S, Stevens B, Ament F, Crewell S, Delanoe J, D Farrell et al (2017) Eurec4a: a field campaign to elucidate the couplings between clouds, convection and circulation. *Surv Geophys* <https://doi.org/10.1007/s10712-017-9428-0>
- Bryan GH, Parker MD (2010) Observations of a squall line and its near environment using high-frequency rawinsonde launches during VORTEX2. *Mon Weather Rev* 138(11):4076–4097. <https://doi.org/10.1175/2010MWR3359.1>
- Burleyson CD, de Szoek SP, Yuter SE, Wilbanks M, Brewer WA (2013) Ship-based observations of the diurnal cycle of southeast pacific marine stratocumulus clouds and precipitation. *J Atmos Sci* 70(12):3876–3894. <https://doi.org/10.1175/JAS-D-13-01.1>
- Chen S, Kerns B, Guy N, Jorgensen D, Delanoe J, Viltard N, Zappa C, Judt F, Lee C, Savarin A (2016) Aircraft observations of dry air, ITCZ, convective cloud systems and cold pools in MJO during DYNAMO. *Bull Am Meteorol Soc.* <https://doi.org/10.1175/bams-d-13-00196.1>
- Ciesielski P, Johnson RH, Jiang X, Zhang Y, Xie S (2017) Relationships between radiation, clouds, and convection during DYNAMO. *J Geophys Res.* <https://doi.org/10.1002/2016JD025965>
- de Szoek S, Skyllingstad ED, Zuidema P, Chandra A (2017) Cold pools and their influence on the tropical marine boundary layer. *J Atmos Sci.* <https://doi.org/10.1175/jas-d-16-0264.1>
- Del Genio AD, Wu J, Wolf AB, Chen Y, Yao MS, Kim D (2015) Constraints on cumulus parameterization from simulations of observed MJO events. *J Clim* 28(16):6419–6442. <https://doi.org/10.1175/JCLI-D-14-00832.1>
- Drager AJ, van den Heever SC (2017) Characterizing convective cold pools. *J. Adv. Model Earth Syst.* <https://doi.org/10.1002/2016MS000788>
- Emanuel KA, Neelin JD, Bretherton CS (1994) On large-scale circulations in convecting atmospheres. *Q J R Meteorol Soc* 120:1111–1143
- Feingold G, Stevens B, Cotton WR, Frisch AS (1996) The relationship between drop in-cloud residence time and drizzle production in numerically simulated stratocumulus clouds. *J Atmos Sci* 53:1108–1122
- Feingold G, Koren I, Wang H, Xue H, Brewer WA (2010) Precipitation-generated oscillations in open cellular cloud fields. *Nature* 466:849–852. <https://doi.org/10.1038/nature09314>
- Feng Z, McFarlane SA, Schumacher C, Ellis S, Comstock J, Bharadwaj N (2014) Constructing a merged cloud-precipitation radar dataset for tropical convective clouds during the DYNAMO/AMIE experiment at Addu Atoll. *J Atmos Ocean Technol* 31:1021–1042
- Feng Z, Hagos S, Rowe AK, Burleyson CD, Martini MN, de Szoek SP (2015) Mechanisms of convective cloud organization by cold pools over tropical warm ocean during the amie/dynamo field campaign. *J Adv Model Earth Syst.* <https://doi.org/10.1002/2014MS000384>
- Flamant C, Knippertz P, Parker DJ, Chaboureaud JP, Lavaysse C, Agusti-Panareda A, Kergoat L (2009) The impact of a mesoscale convective system cold pool on the northward propagation of the intertropical discontinuity over west africa. *Q J R Meteorol Soc* 135:139–159. <https://doi.org/10.1002/qj.357>
- Fragoso AT, Patterson MD, Wettlaufer JS (2013) Mixing in gravity currents. *J Fluid Mech.* <https://doi.org/10.1017/jfm.2013.475>
- Gentine P, Garelli A, Park SB, Nie J, Torri G, Kuang Z (2016) Role of surface heat fluxes underneath cold pools. *Geophys Res Lett* 43(2):874–883. <https://doi.org/10.1002/2015GL067262>
- Glickman T (2000) Glossary of meteorology, 2nd edn. AMS, Flensburg, p 855
- Grandpeix JY, Lafore JP (2010) A density current parameterization coupled with Emanuel’s convection scheme. Part I: the models. *J Atmos Sci.* <https://doi.org/10.1175/2009jas3044.1>
- Grandpeix JY, Lafore JP, Cheruy F (2010) A density current parameterization coupled with Emanuel’s convection scheme. Part II: 1D simulations. *J Atmos Sci* 67(4):898–922. <https://doi.org/10.1175/2009JAS3045.1>
- Grant L, van den Heever S (2016) Cold pool dissipation. *J Geophys Res* 121(3):1138–1155. <https://doi.org/10.1002/2015JD023813>
- Grant LD, van den Heever S (2015) Cold pool and precipitation responses to aerosol loading: modulation by dry layers. *J Atmos Sci* 72:1398–1408
- Hacker J, Linden P, Dalziel S (1996) Mixing in lock-release gravity currents. *Dyn Atmos Oceans* 24(1):183–195. [https://doi.org/10.1016/0377-0265\(95\)00443-2](https://doi.org/10.1016/0377-0265(95)00443-2)
- Hallworth MA, Huppert HE, Phillips JC, Sparks RSJ (1996) Entrainment into two-dimensional and axisymmetric turbulent gravity currents. *J Fluid Mech* 308:289–311. <https://doi.org/10.1017/S0022112096001486>
- Hannah WM, Mapes B, Elsaesser G (2016) A lagrangian view of moisture dynamics during DYNAMO. *J Atmos Sci* 73:1967–1985. <https://doi.org/10.1175/jas-d-15-0243.1>
- Held IM, Hemler RS, Ramaswamy V (1993) Radiative-convective equilibrium with explicit two-dimensional moist convection. *J Atmos Sci* 50(23):3909–3927

- Hohenegger C, Bretherton CS (2011) Simulating deep convection with a shallow convection scheme. *Atmos Chem Phys* 11(20):10389–10406. <https://doi.org/10.5194/acp-11-10389-2011>
- Holloway CE, Wing AA, Bony S, Muller C, Masunaga H, L'Ecuyer T, Turner D, Zuidema P (2017) Observing convective aggregation. *Rev Geophys* 131:780
- Houze RA, Betts A (1981) Convection in GATE. *Rev Geophys Space Phys* 19:541–576
- James RP, Markowski PM (2010) A numerical investigation of the effects of dry air aloft on deep convection. *Mon Weather Rev* 138:140–161. <https://doi.org/10.1175/2009MWR3018.1>
- Jeevanjee N, Romps DM (2013) Convective self-aggregation, cold pools, and domain size. *Geophys Res Lett* 40:994–998. <https://doi.org/10.1002/grl.50204>
- Jeevanjee N, Romps DM (2015) Effective buoyancy, inertial pressure, and the mechanical generation of boundary layer mass flux by cold pools. *J Atmos Sci* 72(8):3199–3213. <https://doi.org/10.1175/JAS-D-14-0349.1>
- Jensen JB, Lee S, Krummel PB, Katzfey J, Gogoasa D (2000) Precipitation in marine cumulus and stratocumulus. Part I: thermodynamic and dynamic observations of closed cell circulations and cumulus bands. *Atmos Res* 54:117–155
- Kazil J, Feingold G, Wang H, Yamaguchi T (2014) On the interaction between marine boundary layer cellular cloudiness and surface heat fluxes. *Atmos Chem Phys* 14(1):61–79. <https://doi.org/10.5194/acp-14-61-2014>
- Khairoutdinov M, Randall D (2006) High-resolution simulations of shallow- to-deep convection transition over land. *J Atmos Sci* 63:3421–3436
- Kiemle C, Gro S, Wirth M, Bugliari L (2017) Airborne lidar observations of water vapor variability in tropical shallow convective environment. *Surv Geophys*. <https://doi.org/10.1007/s10712-017-9431-5>
- Kilpatrick TJ, Xie SP (2015) ASCAT observations of downdrafts from mesoscale convective systems. *Geophys Res Lett* 42:1951–1958. <https://doi.org/10.1002/2015GL063025>
- Kingsmill DE, Houze RA (1999) Thermodynamic characteristics of air flowing into and out of precipitating convection over the west Pacific warm pool. *Q J R Meteorol Soc* 125:1209–1229
- Langhans W, Romps DM (2015) The origin of water vapor rings in tropical oceanic cold pools. *Geophys Res Lett* 42:7824–7834. <https://doi.org/10.1002/2015GL065623>
- LeMone MA (1980) On the difficulty of measuring temperature and humidity in cloud: comments on “Shallow convection on day 261 of GATE: Mesoscale arcs”. *Mon Weather Rev* 108:1702–1705
- LeMone MA, Pennell WT (1976) The relationship of trade wind cumulus distribution to subcloud layer fluxes and structure. *Mon Weather Rev* 104:524–539
- Leon D, Wang Z, Liu D (2008) Climatology of drizzle in marine boundary layer clouds based on one year of data from CloudSat and CALIPSO. *J Geophys Res*. <https://doi.org/10.1029/2008JD009835>
- Li Z, Zuidema P, Zhu P (2014) Simulated convective invigoration processes at trade-wind cumulus cold pool boundaries. *J Atmos Sci* 71:2823–2841. <https://doi.org/10.1175/JAS-D-13-0184.1>
- Li Z, Zuidema P, Zhu P, Morrison H (2015) The sensitivity of simulated shallow cumulus convection and cold pools to microphysics. *J Atmos Sci* 72:3340–3355. <https://doi.org/10.1175/JAS-D-14-0099.1>
- Mapes B, Chandra A, Kuang Z, Zuidema P (2017) Importance profiles for water vapor. *Surv Geophys*. <https://doi.org/10.1007/s10712-017-9427-1>
- Markowski PM, Richardson YP (2014) The influence of environmental low-level shear and cold pools on tornadogenesis: insights from idealized simulations. *J Atmos Sci* 71(1):243–275. <https://doi.org/10.1175/JAS-D-13-0159.1>
- Mechem D, Yuter SE, de Szoeke SP (2012) Thermodynamic and aerosol controls in southeast pacific stratocumulus. *J Atmos Sci* 69:1250–1266. <https://doi.org/10.1175/JAS-D-11-0165.1>
- Medeiros B, Nuijens L, Antoniazzi C, Stevens B (2010) Lowlatitude boundary layer clouds as seen by CALIPSO. *J Geophys Res*. <https://doi.org/10.1029/2010JD014437>
- Muller C, Bony S (2015) What favors convective aggregation and why? *Geophys Res Lett* 42:5626–5634. <https://doi.org/10.1002/2015gl064260>
- Muller CJ, Held IM (2012) Detailed investigation of the self-aggregation of convection in cloud-resolving simulations. *J Atmos Sci* 69:2551–2565. <https://doi.org/10.1175/JAS-D-11-0257.1>
- Nair US, Weger RC, Kuo KS, Welch RM (1998) Clustering, randomness, and regularity in cloud fields. 5. The nature of regular cumulus cloud fields. *J Geophys Res* 103:11,363–11,380
- Neggers RA, Siebesma AP, Jonker HJJ (2002) A multiparcel model for shallow cumulus convection. *J Atmos Sci* 59:1655–1667
- Nitta T, Esbensen S (1974) Heat and moisture budget analyses using BOMEX data. *Mon Weather Rev* 102:17–28
- Nolan DS, Tulich SN, Blanco JE (2016) ITCZ structure as determined by parameterized versus explicit convection in aquachannel and aquapatch simulations. *J Adv Model Earth Syst* 8:425–452. <https://doi.org/10.1002/2015MS000560>



- Nuijens L, Medeiros B, Sandu I, Ahlgrimm M (2015) The behavior of trade-wind cloudiness in observations and models: the major cloud components and their variability. *J Adv Model Earth Syst* 7(2):600–616. <https://doi.org/10.1002/2014MS000390>
- Nuijens L, Emanuel K, Masunaga H, L'Ecuyer T (2017) Implications for warm rain in shallow cumulus and congestus clouds for large-scale circulations. *Surv Geophys*. <https://doi.org/10.1007/s10712-017-9429-z>
- Pantillon F, Knippertz P, Marsham JH, Birch CE (2015) A parameterization of convective dust storms for models with mass-flux convection schemes. *J Atmos Sci* 72(6):2545–2561. <https://doi.org/10.1175/JAS-D-14-0341.1>
- Qian L, Young GS, Frank WM (1998) A convective wake parameterization scheme for use in general circulation models. *Mon Weather Rev* 126(2):456–469. [https://doi.org/10.1175/1520-0493\(1998\)126%3c0456:ACWPSF%3e2.0.CO;2](https://doi.org/10.1175/1520-0493(1998)126%3c0456:ACWPSF%3e2.0.CO;2)
- Rauber RM et al. (2007) Rain in shallow cumulus over the ocean: the RICO campaign. *Bull Am Meteorol Soc* 88:1912–1928
- Raymond D (1995) Regulation of moist convection over the west pacific warm pool. *J Atmos Sci* 52:3945–3959
- Riehl H, Yeh C, Malkus J, Seur NL (1951) The northeast trade of the Pacific ocean. *Q J R Meteorol Soc* 77:598–626
- Riley EM, Mapes BE, Tulich SN (2011) Clouds associated with the Madden-Julian oscillation: a new perspective from CloudSat. *J Atmos Sci* 68(12):3032–3051. <https://doi.org/10.1175/JAS-D-11-030.1>
- Rio C, Hourdin F, Grandpeix JY, Lafore JP (2009) Shifting the diurnal cycle of parameterized deep convection over land. *Geophys Res Lett*. <https://doi.org/10.1029/2008GL036779>
- Rio C, Grandpeix JY, Hourdin F, Guichard F, Couvreur F, Lafore JP, Fridlind A, Mrowiec A, Roehrig R, Rochetin N, Lefebvre MP, Idelkadi A (2013) Control of deep convection by sub-cloud lifting processes: the alp closure in the lmdz5b general circulation model. *Clim Dyn* 40(9):2271–2292. <https://doi.org/10.1007/s00382-012-1506-x>
- Romps DM, Jeevanjee N (2016) On the sizes and lifetimes of cold pools. *Q J R Meteorol Soc* 142(696):1517–1527
- Ross AN, Tompkins AM, Parker DJ (2004) Simple models of the role of surface fluxes in convective cold pool evolution. *J Atmos Sci* 61(13):1582–1595. [https://doi.org/10.1175/1520-0469\(2004\)061%3c1582:SMOTRO%3e2.0.CO;2](https://doi.org/10.1175/1520-0469(2004)061%3c1582:SMOTRO%3e2.0.CO;2)
- Rotunno R, Klemp JB, Weisman ML (1988) A theory for strong, long-lived squall lines. *J Atmos Sci* 45:463–485. [https://doi.org/10.1175/1520-0469\(1988\)045%3c0463:ATFSSL%3e2.0.CO;2](https://doi.org/10.1175/1520-0469(1988)045%3c0463:ATFSSL%3e2.0.CO;2)
- Rowe AK, Houze RA (2015) Cloud organization and growth during the transition from suppressed to active MJO convection. *J Geophys Res* 120:10,324–10,350. <https://doi.org/10.1002/2014JD022948>
- Rozbicki JJ, Young GS, Qian L (1999) Test of a convective wake parameterization in the single-column version of ccm3. *Mon Weather Rev* 127(6):1347–1361. [https://doi.org/10.1175/1520-0493\(1999\)127%3c1347:TOACWP%3e2.0.CO;2](https://doi.org/10.1175/1520-0493(1999)127%3c1347:TOACWP%3e2.0.CO;2)
- Ruppert JH, Johnson RH (2015) Diurnally modulated cumulus moistening in the preonset stage of the Madden-Julian oscillation during dynamo. *J Atmos Sci* 72:1622–1647. <https://doi.org/10.1175/JAS-D-14-0218.1>
- Savic-Jovicic V, Stevens B (2008) The structure and mesoscale organization of precipitating stratocumulus. *J Atmos Sci* 65:1587–1605. <https://doi.org/10.1175/2007JAS2456.1>
- Saxen TR, Rutledge SA (1998) Surface fluxes and boundary layer recovery in TOGA COARE: sensitivity to convective organization. *J Atmos Sci* 55:2763–2781
- Schiro KA, Neelin JD (2017) Tropical continental downdraft characteristics: mesoscale systems versus unorganized convection. *Atmos Chem Phys Discuss* 2017:1–29. <https://doi.org/10.5194/acp-2017-684>
- Schlemmer L, Hohenegger C (2014) The formation of wider and deeper clouds as a result of cold-pool dynamics. *J Atmos Sci* 71:2842–2858. <https://doi.org/10.1175/JAS-D-13-0170.1>
- Schlemmer L, Hohenegger C (2016) Modifications of the atmospheric moisture field as a result of cold-pool dynamics. *Q J R Meteorol Soc* 142:30–42. <https://doi.org/10.1002/qj2625>
- Schubert W (1995) Dynamical adjustment of the trade-wind inversion layer. *J Atmos Sci* 52:2941–2952
- Seifert A, Heus T (2013) Large-eddy simulation of organized precipitating trade-wind cumulus clouds. *Atmos Chem Phys* 13:5631–5645. <https://doi.org/10.5194/acp-13-5631-2013>
- Sherwood SC, Roca R, Weckwerth TM, Andronova NG (2010) Tropospheric water vapor, convection, and climate. *Rev Geophys*. <https://doi.org/10.1029/2009RG000301>
- Siebesma AP, Bretherton CS, Brown BA, Chlond A, Cuxart J, Duynkerke P, Jiang H, Khairoutdinov M, Lewellen D, Moeng CH, Sanchez E, Stevens B, Stevens DE (2003) A large-eddy simulation study of shallow cumulus convection. *J Atmos Sci* 60:1201–1219
- Snodgrass ER, Girolamo LD, Rauber RM (2009) Precipitation characteristics of trade wind clouds during RICO derived from radar, satellite, and aircraft measurements. *J Appl Meteorol Clim* 48:464–483

- Srivastava RC (1987) A model of intense downdrafts driven by the melting and evaporation of precipitation. *J Atmos Sci* 44:1752–1774
- Stevens B, Farrell D, Hirsch L, Jansen F, Nuijens L, Serikov I, Uggemann BB, Forde M, Linne H, Lonitz K, Prospero J (2016) The Barbados cloud observatory: anchoring investigations of clouds and circulation on the edge of the ITCZ. *Bull Am Meteorol Soc* 97:787–801. <https://doi.org/10.1175/BAMS-D-14-00247.1>
- Stevens B, Brogniez H, Kiemle C, Lacour JL, Crevoisier C, Kiliani J (2017) Structure and dynamical influence of water vapor in the lower tropical troposphere. *Surv Geophys*. <https://doi.org/10.1007/s10712-017-9420-8>
- Takemi T, Satomura T (2000) Numerical experiments on the mechanisms for the development and maintenance of long-lived squall lines in dry environments. *J Atmos Sci* 57:1718–1740
- Takemi T, Hirayama O, Liu C (2004) Factors responsible for the vertical development of tropical oceanic cumulus convection. *Geophys Res Lett*. <https://doi.org/10.1029/2004GL020225>
- Terai C, Wood R (2013) Aircraft observations of cold pools under marine stratocumulus. *Atmos Chem Phys* 13:9899–9914. <https://doi.org/10.5194/acp-13-9899-2013>
- Thayer-Calder K, Randall D (2015) A numerical investigation of boundary layer quasi-equilibrium. *Geophys Res Lett* 42:550–556. <https://doi.org/10.1002/2014GL062649>
- Tobin I, Bony S, Roca R (2012) Observational evidence for relationships between the degree of aggregation of deep convection, water vapor, surface fluxes, and radiation. *J Clim* 25:6885–6904
- Tompkins AM (2001) Organization of tropical convection in low vertical wind shears: the role of cold pools. *J Atmos Sci* 58:1650–1672
- Tompkins AM, Semie AG (2017) Organization of tropical convection in low vertical wind shears: role of updraft entrainment. *J Adv Model Earth Syst* 9:1046–1068. <https://doi.org/10.1002/2016MS000802>
- Torri G, Kuang Z (2016a) A lagrangian study of precipitation-driven downdrafts. *J Atmos Sci*. <https://doi.org/10.1175/JAS-D-15-0222s1>
- Torri G, Kuang Z (2016b) Rain evaporation and moist patches in tropical boundary layers. *Geophys Res Lett* 43:9895–9902. <https://doi.org/10.1002/2016GL070893>
- Torri G, Kuang Z, Tian Y (2015) Mechanisms for convection triggering by cold pools. *Geophys Res Lett* 42(6):1943–1950. <https://doi.org/10.1002/2015GL063227>
- Trzeciak TM, Garcia-Carreras L, Marsham JH (2017) Cross-saharan transport of water vapor via recycled cold pool outflows from moist convection. *Geophys Res Lett* 44:1554–1563. <https://doi.org/10.1002/2016GL072108>
- van Zanten MC, Stevens B (2005) Observations of the structure of heavily precipitating marine stratocumulus. *J Atmos Sci* 62:4327–4342
- van Zanten MC, Stevens B, Nuijens L, Siebesma AP, Ackerman A, Burnet F, Cheng A, Couvreux F, Jiang H, Khairoutdinov M, Kogan Y, Lewellen DC, Mechem D, Nakamura K, Noda A, Shipway BJ, Slawinska J, Wang S, Wyszogrodzki A (2011) Controls on precipitation and cloudiness in simulations of trade-wind cumulus as observed during RICO. *J Adv Model Earth Syst*. <https://doi.org/10.1029/2011MS000056>
- Vogel R, Nuijens L, Stevens B (2016) The role of precipitation and spatial organization in the response of trade-wind clouds to warming. *J Adv Model Earth Syst* 8:843–862. <https://doi.org/10.1002/2015MS000568>
- Wang H, Feingold G (2009) Modeling mesoscale cellular structure and drizzle in marine stratocumulus. Part I: impact of drizzle on the formation and evolution of open cells. *J Atmos Sci* 66:3237–3256. <https://doi.org/10.1175/2009JAS3022.1>
- Wang S, Sobel A, Fridlind A, Feng Z, Comstock J, Minnis P, Nordeen M (2015) Simulations of cloud-radiation interaction using large-scale forcing derived from the CINDY/DYNAMO northern sounding array. *J Adv Model Earth Syst* 7(3):1472–1498. <https://doi.org/10.1002/2015MS000461>
- Warner C, Simpson J, Martin DW, Suchman D, Mosher FR, Reinking RF (1979) Shallow convection on day 261 of GATE: mesoscale arcs. *Mon Weather Rev* 107:1617–1635
- Wilbanks M, Yuter SE, deZoeke SP, Brewer WA, Miller MA, Hall AM, Burleyson CD (2015) Near-surface density currents observed in the southeast pacific stratocumulus-topped marine boundary layer. *Mon Weather Rev* 143:3532–3555
- Wing AA, Emanuel K, Holloway C, Muller C (2017) Convective self-aggregation in numerical simulations: a review. *Surv Geophys*. <https://doi.org/10.1007/s10712-017-9408-4>
- Wood R (2005a) Drizzle in stratiform boundary layer clouds. Part I: vertical and horizontal structure. *J Atmos Sci* 62:3012–3033
- Wood R (2005b) Drizzle in stratiform boundary layer clouds. Part II: microphysical aspects. *J Atmos Sci* 62:3034–3050

- Wood R, Bretherton CS, Leon D, Clarke AD, Zuidema P, Allen G, Coe H (2011) An aircraft case study of the spatial transition from closed to open mesoscale cellular convection over the Southeast Pacific. *Atmos Chem Phys* 11:2341–2370. <https://doi.org/10.5194/acp-11-2341-2011>
- Xue H, Feingold G, Stevens B (2008) Aerosol effects on clouds, precipitation, and the organization of shallow cumulus convection. *J Atmos Sci* 65:392–406. <https://doi.org/10.1175/2007JAS2428.1>
- Yamaguchi T, Feingold G, Kazil J, McComiskey A (2015) Stratocumulus to cumulus transition in the presence of elevated smoke layers. *Geophys Res Lett*. <https://doi.org/10.1002/2015GL066544>
- Yoneyama K, Zhang C, Long CN (2013) Tracking pulses of the Madden–Julian oscillation. *Bull Am Meteorol Soc* 94:1871–1891. <https://doi.org/10.1175/bams-d-12-00157.1>
- Young GS, Perugini SM, Fairall CW (1995) Convective wakes in the equatorial western Pacific during TOGA. *Mon Weather Rev* 123:110–123
- Zhang J, Zuidema P, Turner DD, Cadeddu MP (2017) Tropical humidity vertical structure inferred from a microwave radiometer during dynamo. *J Appl Meteor Clim (Under review)*
- Zhou X, Heus T, Kollias P (2017) Influences of drizzle on stratocumulus cloudiness and organization. *J Geophys Res* 122(13):6989–7003. <https://doi.org/10.1002/2017JD026641>
- Zipser E (1977) Mesoscale and convective-scale downdrafts as distinct components of squall line structure. *Mon Weather Rev* 105:1568–1589
- Zuidema P (1998) The 600–800-mb minimum in tropical cloudiness observed during TOGA COARE. *J Atmos Sci* 55:2220–2228
- Zuidema P, Painemal D, deSzoeko S, Fairall C (2009) Stratocumulus cloud top height estimates and their climatic implications. *J Clim* 22:4652–4666
- Zuidema P, Li Z, Hill R, Bariteau L, Rilling B, Fairall C, Brewer WA, Albrecht B, Hare J (2012) On trade-wind cumulus cold pools. *J Atmos Sci* 69:258–277. <https://doi.org/10.1175/jas-d-11-0143.1>
- Zuidema P, Redemann J, Haywood J, Wood R, Piketh S, Hipondoka M, Formenti P (2016) Smoke and clouds above the southeast atlantic: upcoming field campaigns probe absorbing aerosol's impact on climate. *Bull Am Meteorol Soc* 97:1131–1135. <https://doi.org/10.1175/bams-d-15-00082.1>